

The influence of the platinum substrate roughness on the ferroelectric properties of $0.65\text{Pb}(\text{Mg}_{1/3}\text{Nb}_{2/3})\text{O}_3-0.35\text{PbTiO}_3$ thick films

Hana Uršič^{1,2}, Elena Tchernychova¹, Andreja Benčan^{1,2}, Jenny Jouin¹, Janez Holc^{1,2}, Silvo Drnovšek^{1,2}, Marko Hrovat^{1,2}, Barbara Malič¹

¹Electronic Ceramics Department, Jožef Stefan Institute, Ljubljana, Slovenia

²Centre of Excellence NAMASTE, Ljubljana, Slovenia

Abstract: The $0.65\text{Pb}(\text{Mg}_{1/3}\text{Nb}_{2/3})\text{O}_3-0.35\text{PbTiO}_3$ thick films were screen-printed on conductive platinum substrates, which differed in the surface roughness for almost an order of magnitude, namely, the vertical root mean square roughness values, determined by atomic force microscopy, were 44 nm and 342 nm, respectively. The films, sintered at 950 °C, crystallized in monoclinic and tetragonal perovskite phases, however, the film on the flat Pt substrate exhibited a higher degree of the (001) orientation of the tetragonal phase, and also a higher remnant polarization than the film on the rough Pt substrate. Transmission electron microscope analysis revealed the presence of an interfacial Pb-Pt phase between the film and the substrate, which was in the form of a continuous layer on the flat substrate, while on the rough Pt-substrate, it was segregated in surface imperfections. The appearance of the intermetallic phase at the film-substrate interface was attributed to the transient reducing atmosphere generated in the thick film upon heating as a consequence of thermal decomposition of organic screen-printing additives. This work confirms the importance of the substrate roughness in regard to the functional properties of the films.

This work is dedicated to the late Professor Marija Kosec

Keywords: 0.65PMN-0.35PT, thick film, platinum substrate, roughness, ferroelectric properties

Vpliv hrapavosti platinske podlage na feroelektrične lastnosti debelih plasti $0.65\text{Pb}(\text{Mg}_{1/3}\text{Nb}_{2/3})\text{O}_3-0.35\text{PbTiO}_3$

Izvleček: Debele plasti $0.65\text{Pb}(\text{Mg}_{1/3}\text{Nb}_{2/3})\text{O}_3-0.35\text{PbTiO}_3$ so bile z metodo sitotiska nanesene na prevodne platinske podlage, ki so se razlikovale v hrapavosti površine za skoraj velikostni red, in sicer je bila vertikalna srednja vrednost hrapavosti (koren srednjih kvadratov - rms), ki smo jo določili z mikroskopom na atomsko silo, 44 nm in 342 nm. Plasti, sintrane pri 950 °C, kristalizirajo v monoklinski in tetragonalni perovskitni fazi, vendar plasti na ravni Pt-podlagi izkazujejo višjo stopnjo (001) usmerjenosti tetragonalne faze, prav tako pa tudi višjo remanentno polarizacijo, kot plasti na hrapavi Pt-podlagi. Analiza, narejena s presežno elektronsko mikroskopijo, je razkrila prisotnost intermetalne faze Pb-Pt med debelo plastjo in platinsko podlago, ki je bila na ravni podlagi prisotna v obliki neprekinjene plasti, medtem ko je bila na podlagi z veliko hrapavostjo segregirana v otočke. Pojav intermetalne faze na meji plast-podlaga pripisujemo prehodni redukcijski atmosferi, ki nastane v debelih plasteh med segrevanjem zaradi termičnega razpada organskih dodatkov v pasti za sitotisk. V članku je prikazan velik vpliv hrapavosti podlage na funkcijske lastnosti debelih plasti.

Ključne besede: 0.65PMN-0.35PT, debela plast, platinska podlaga, hrapavost, feroelektrične lastnosti

*Corresponding Author's e-mail: hana.ursic@ijs.si

1 Introduction

Relaxor-ferroelectrics, including the solid solution of $\text{Pb}(\text{Mg}_{1/3}\text{Nb}_{2/3})\text{O}_3-\text{PbTiO}_3$ (PMN-PT) as the prototype

material, are characterized by a high dielectric permittivity, high electrostrictive and high piezoelectric properties and may be used for applications such as sensors, actuators, ultrasonic medical diagnostics and

non-destructive testing [1–3]. Several applications require films with the thicknesses in a range of few μm to a few 10 μm , and screen-printing is a simple, convenient and low-cost method for producing them.

Recently, bending-type actuators with large-displacement, consisting of the $0.65\text{Pb}(\text{Mg}_{1/3}\text{Nb}_{2/3})\text{O}_3-0.35\text{PbTiO}_3$ (0.65PMN–0.35PT) thick-film on a thin Pt support, were designed. The preparation of such thick-film actuators is not trivial. After screen printing the film on a bulk platinumized alumina substrate and subsequent firing, the 0.65PMN–0.35PT/Pt structure needs to be removed from the stiff substrate. The performance of such self-standing 0.65PMN–0.35PT/Pt actuator is excellent, i.e., the displacements of nearly 100 μm have been achieved for actuators with the dimensions of 18 mm \times 2.5 mm \times 50 μm at only 18 V, which is five times larger as compared to the displacement of similar actuators described in the literature [4]. A future trend is to pattern the thick-film by printing directly on a thin Pt foil, which acts both as the substrate and as the bottom electrode. For successful design of such actuators, the influence of the surface conditions of the Pt-support on the properties of the active thick film needs to be understood.

In this work two substrates with different surface roughnesses were used and their influence on the structure and ferroelectric properties of the 0.65PMN–0.35PT thick films was compared. The first one was an optically-polished platinum block, while the second one was prepared by screen printing the platinum paste on such block and firing at 1200 $^\circ\text{C}$, resulting in a much higher surface roughness. Such screen-printed bottom electrodes are typically deposited on alumina or Low Temperature Cofired Ceramic (LTCC) substrates. By introducing a screen-printed Pt-layer on top of the Pt-block our aim has been to: i) mimic the configuration of a typical screen-printed thick film structure and thus to achieve similar film/substrate interface conditions, however, ii) by using the platinum block as the substrate to keep the same level of thermal stresses in both thick film structures. The influence of the roughness of the Pt-substrate on the structural and ferroelectric properties of 0.65PMN–0.35PT thick films is discussed.

2 Experimental

For the synthesis of $0.65\text{Pb}(\text{Mg}_{1/3}\text{Nb}_{2/3})\text{O}_3-0.35\text{PbTiO}_3$ (0.65PMN–0.35PT) a mixture of PbO (99.9%, Aldrich), MgO (98%, Aldrich), TiO_2 (99.8%, Alfa Aesar) and Nb_2O_5 (99.9%, Aldrich) in the stoichiometric molar ratio with an excess of 2 mol% PbO was high-energy milled in a

planetary mill (Retsch, Model PM 400). After milling, the powder was heated at 700 $^\circ\text{C}$ for 1 h, milled in an attritor mill in i-propanol, dried and sieved. More details about mechanochemical activation of 0.65PMN–0.35PT powder are described in [5–8].

The 2-mm-thick platinum substrates were obtained from Zlatarna Celje (Pt 999). A Pt paste (Ferro 6412) was screen-printed and fired at 1200 $^\circ\text{C}$ for 1 h on Pt substrate. The thickness of the printed layer was around 10 μm . In further text, the substrates are denoted as Pt-flat and Pt-rough, respectively.

The 0.65PMN–0.35PT thick-film paste was prepared from a mixture of the prereacted powder and an organic vehicle, consisting of alpha-terpineol, [2-(2-butoxy-ethoxy)-ethyl]-acetate and ethyl cellulose in the ratio 60/25/15. The paste was printed on both substrates four times with intermediate drying at 150 $^\circ\text{C}$. The samples were heated at 500 $^\circ\text{C}$ for 1 h to decompose the organic vehicle, and sintered at 950 $^\circ\text{C}$ for 2 h in PbZrO_3 packing powder with an excess of 2 mol% PbO and then cooled to room temperature with a rate of 3 $^\circ\text{C}/\text{min}$. The thicknesses of the films were around 40 μm . A fourfold printing of the paste (i.e., 40 μm of final thickness) is an optimal choice to study film properties. A single printed layer is not sufficiently uniform, while in films thicker than 100 μm , cracks would appear during thermal treatment.

The sintered films were analysed by PANalytical X'Pert PRO MPD X-ray diffractometer using $\text{Cu K}\alpha_1$ radiation ($\lambda = 1.54051 \text{ \AA}$) from $2\theta = 10^\circ$ to 70° using a step of 0.033° and the time per step of 100 s. The phase composition was determined by the Rietveld analysis using the Jana2006 software [9]. The starting unit-cell parameters and the atomic positions for the 0.65PMN–0.35PT were taken from a former Rietveld study by Singh et al. [10].

The cross-section samples were prepared for microstructural analysis. The samples were mounted in epoxy, ground and polished using standard metallographic techniques. The microstructures of the samples were investigated by a field emission scanning electron microscopy (FE-SEM, Supra 35 VP, Carl Zeiss) by secondary electrons. The digitalized microstructures were processed with the Image Tool software14 (UTH-SCSA Image Tool Version 3.00, 2002) to obtain the areas consisting of more than 120 grains. The grain size was expressed as the Feret's diameter (d_f).

The cross-section microstructures were also analysed by analytical transmission electron microscope (TEM, JEM 2010F, JEOL) equipped with an Energy-Dispersive X-ray spectrometer (EDXS). The samples were prepared conventionally by mounting the thick-film structures

with the epoxy glue into the sandwich, which was then ground, polished, dimpled and finally Ar⁺-ion milled until perforation.

The topography and the root mean square (rms) vertical roughness of both Pt substrates were analyzed by the atomic force microscope (AFM, Asylum Research, Molecular Force Probe 3D). A tetrahedral non-coated Si tip on a Si cantilever coated by Al was used for the contact-mode imaging with the typical spring constant of 2 N/m.

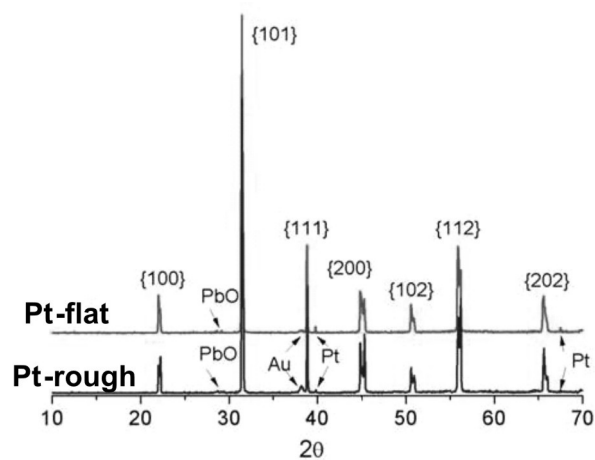
The 0.65PMN–0.35PT thick-film paste, dried at 150 °C to constant mass, was analysed by the thermogravimetric and differential thermal analysis (TG/DTA, Netzsch STA 409C). The sample with the mass of about 50 mg, deposited in an Al₂O₃ crucible, was analysed upon heating from 30 °C to 650 °C with the heating rate of 10 K min⁻¹ in the flowing synthetic air (80 % N₂ – 20 % O₂) atmosphere.

For ferroelectric measurements, Au/Cr electrodes with a 1.5-mm diameter were deposited by magnetron sputtering (BAL-TEC SCD 005) on the top surface of the films. The ferroelectric hysteresis loops were measured by the Aixacct TF Analyser 2000 and the high voltage amplifier TREK 609E-6 at 50 Hz.

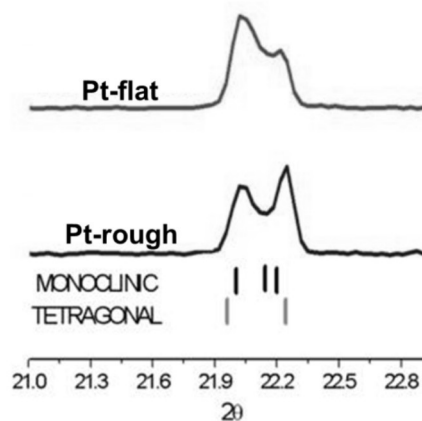
3 Results

The X-ray diffraction diagrams (XRD) for 0.65PMN–0.35PT thick films on the Pt-flat and Pt-rough substrates, prepared under the same conditions, reveal the presence of the perovskite phase, see Figure 1a. No extra reflections, which might correspond to the pyrochlore phase, were observed. Low-intensity diffraction peaks of PbO were detected in both XRD-patterns. Figure 1b shows the magnified regions of the diffraction patterns which correspond to the family of {100} Bragg peaks.

Although the 0.65PMN–0.35PT films on both substrates were prepared under the same conditions, their XRD patterns are obviously different. For description of the perovskite diffraction patterns the coexistence of monoclinic and tetragonal phases should be considered. Namely, it was shown in our previous work that the phase ratio in the 0.65PMN–0.35PT thick films on different substrates depended on the stress conditions, induced by the choice of the substrate [5]. The amounts of the monoclinic Pm and tetragonal P4mm phases in the two samples were calculated, and they are 81 % ± 1 % and 19 % ± 1 % in both cases. The same phase ratio in both samples indicates that the thermal stresses in both films are the same, in agreement



a.



b.

Figure 1: (a) The XRD diagram of 0.65PMN–0.35PT films on the Pt-flat and Pt-rough substrates. The families of Bragg peaks are written in brackets. The peaks corresponding to top Au and bottom Pt electrodes are marked by arrows; (b) The regions of the diffraction patterns corresponding to the family of {100} Bragg peaks. The refined peak positions of the (0 0 1), (1 0 0) tetragonal (grey, below) and the (0 0 1), (1 0 0), (0 1 0) monoclinic (black, above) phases are marked.

with [5]. When the (001) preferential orientation of the tetragonal phase was included in the Rietveld refinement, the quality of the fit was improved. The reliability factors for the monoclinic Pm (R_M) and tetragonal P4mm (R_T) phases, and the goodness of the fit (GOF) for the 0.65PMN–0.35PT films on Pt-flat and Pt-rough substrates were 3.68, 4.18, 1.10, and 4.05, 5.32, 1.42, respectively.

In a randomly oriented tetragonal perovskite-phase thick film, the number of the a-domains, i.e., with the a-axis in plane of the film, is twice that of the c-domains, i.e., with the polar, c-axis out of plane of the film. Consequently, the ratio of the peak intensities $I_{(001)}/(I_{(100)} + I_{(010)})$

+ $I_{(001)}$) for the non-oriented perovskite phase is 0.33. In our study such ratio was 0.66 and 0.50 for the 0.65PMN–0.35PT films on Pt-flat and Pt-rough substrates, respectively. Thus, in both cases, the preferential c-domain orientation was evidenced, and it was more pronounced in the film on the Pt-flat substrate, reaching twice the value of the randomly oriented phase.

The SEM cross-section microstructures of the 0.65PMN–0.35PT films on both Pt substrates are shown in Figure 2. The films are quite dense. The grain size, d_p , is similar in both films, i.e., $1.1 \mu\text{m} \pm 0.4 \mu\text{m}$ and $1.3 \mu\text{m} \pm 0.5 \mu\text{m}$ for the films on Pt-flat and Pt-rough substrates. The comparison of the PMN–PT/Pt interfaces in Figure 2a and c reveals the flat surface of the polished Pt block in the former case, and a much rougher surface of the screen-printed platinum layer in the latter one.

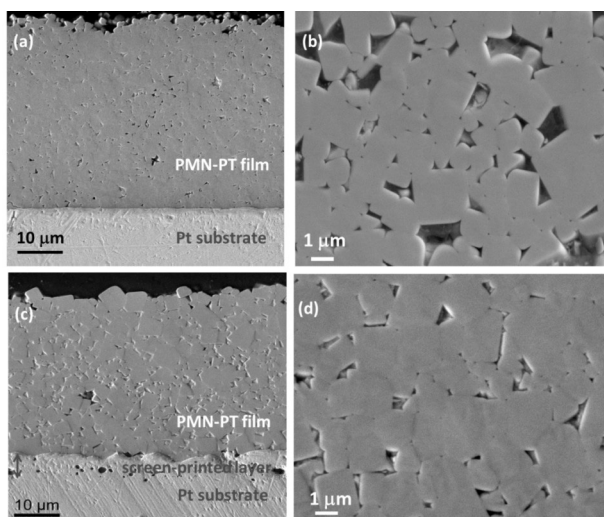


Figure 2: SEM cross-section images of 0.65PMN–0.35PT films on (a), (b) Pt-flat and (c), (d) Pt-rough substrates.

Moreover, the surface roughness of 0.65PMN–0.35PT films on both Pt substrates is determined primarily by the grain size, which is similar in both films. The rms roughness determined by AFM is approximately $0.5 \mu\text{m}$.

The 0.65PMN–0.35PT thick films on both Pt substrates were further examined by the TEM-EDXS analysis. In Figure 3, the bright- and dark-field TEM micrographs of the film/Pt substrate interfaces are shown. In both specimens, an intermetallic Pb–Pt phase was detected at the film/substrate interface. The distributions of the intermetallic Pb–Pt phase at the film/Pt interface were different in the two samples and they could be related to the fractions of the (001) preferential domain orientation in the 0.65PMN–0.35PT thick films. Namely, in the film on the Pt-flat substrate, which showed a higher degree of the (001) preferential orientation, a continuous Pb–Pt layer was formed at the film-substrate interface

(see Figure 3a and c), while in the film on the Pt-rough substrate with a lower degree of the (001) preferential orientation, only rare inclusions of Pb–Pt pockets were detected (Figure 3b and d).

Note that in the film on the Pt-flat substrate an additional layer could be observed between the Pb–Pt phase and 0.65PMN–0.35PT thick film, see Figure 3a. From the electron diffraction analysis we assume that this could be a pyrochlore phase, however a precise analysis of this layer could not be performed.

The intermetallic Pb–Pt phase has been often reported in the studies of lead-based perovskite thin films of various compositions, such as lead zirconate titanate (PZT) [11–17], however, in the thick-film studies it was reported only in the case when the PZT film was deposited on the platinised silicon substrate [18].

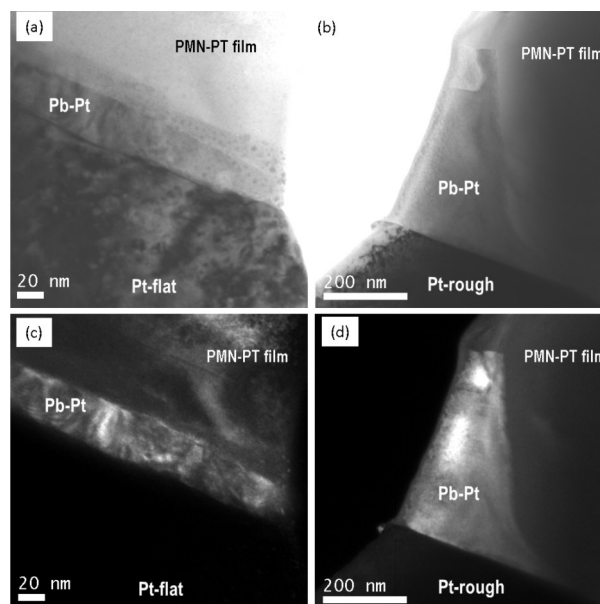


Figure 3: Bright (a), (b) and dark-field (c), (d) TEM micrographs of 0.65PMN–0.35PT films on Pt-flat and Pt-rough substrates.

Similar to PZT or PMN–PT thin-film structures [11–17], the formation of the intermetallic Pb–Pt phase in the thick 0.65PMN–0.35PT films may be attributed to the partial reduction of Pb^{2+} species to metallic lead in the process of the thermal decomposition of the organic vehicle in the 0.65PMN–0.35PT thick film during heating to $500 \text{ }^\circ\text{C}$ in air.

In order to verify the assumption, the thermal analysis of the 0.65PMN–0.35PT thick film paste, dried at $150 \text{ }^\circ\text{C}$, was performed in air, see Figure 4. The sample lost 8.41 weight % upon heating to $450 \text{ }^\circ\text{C}$. The major weight loss of 7.95 % occurred between approximately 200 and $380 \text{ }^\circ\text{C}$, as evident from the thermogravimetric

(TG) and derivative thermogravimetric (DTG) curves, respectively. This weight loss was strongly exothermic, with the differential thermal analysis (DTA) peak at 308 °C. A minor weight loss of about 0.5 % occurred between 380 and 450 °C with the DTG and DTA–exo peaks at 430 °C. The two steps of weight loss are due to thermal decomposition of residual solvent alpha-terpineol, [2-(2-butoxy-ethoxy)-ethyl]-acetate and ethyl cellulose in air. It is reasonable to expect that in the bulk of the powder thermal oxidation of organic species in ambient atmosphere could result in a decreased partial pressure of O₂ to a low enough level to cause transient reduction of Pb²⁺ species to metallic lead, and, as already discussed above, in the thick film, to the formation of a Pb-Pt phase at the film/Pt-substrate interface.

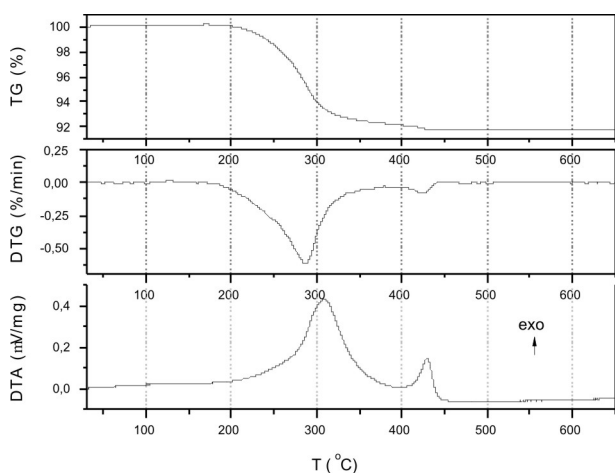


Figure 4: TG, DTG and DTA curves of the 0.65PMN–0.35PT paste, dried at 150 °C, recorded in air.

In solution-derived PZT thin films such Pb-Pt phase was stable upon heating to 350–700 °C, depending on the heating rate [12, 15, 16], and upon further heating in air the metallic lead was reoxidized to Pb²⁺ [12]. Note that the thickness of thin films was a few 100 nm. In the thick 0.65PMN–0.35PT films on Pt-substrates, which were sintered at 950 °C and cooled to room temperature, the Pb-Pt phase was still present. The exact composition of the intermetallic phase could not be determined due to the sputtering of Pt from the substrate during the TEM-specimen preparation. In the Pb-Pt phase diagram [19] three intermetallic compounds are formed, i.e., the Pb₄Pt, which is stable up to 360 °C, the PbPt, which is stable up to 795 °C, and the PbPt₃, which is stable up to 915 °C; and at higher temperatures the liquid phase is formed. We assume that in the case of the 0.65PMN–0.35PT thick film, the lead could not be reoxidized due to the slow diffusion of oxygen through about 40 μm of the film thickness (see Figure 2).

The cross-section microstructures of both 0.65PMN–0.35PT films on Pt-substrates reveal significant differ-

ences in the substrate roughness as evident from Figures 2a and c, respectively. The latter was evaluated on the pristine Pt-substrates by AFM imaging. The topographic AFM image of the Pt-flat substrate reveals a

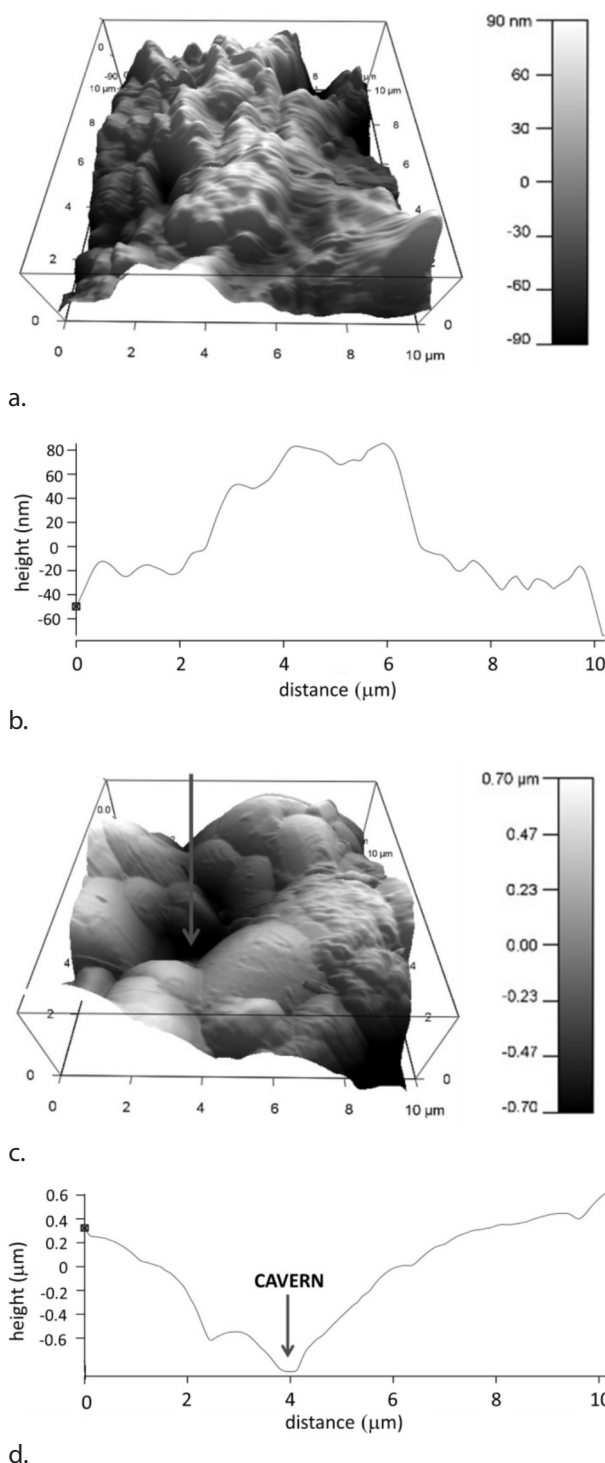


Figure 5: Topographic AFM images and scanning line profiles of the Pt-flat (a, b) and Pt-rough (c, d) substrates. Note the change of scale of the two pairs of images.

smooth surface with the image rms roughness of 44 nm, see Figure 5a. The profile of a selected scanning line is given in Figure 5b. In contrary, the topographic AFM image of the Pt-rough substrate reveals a much rougher surface, with the image rms roughness of 342 nm, see Figure 5c, d, which is almost an order of magnitude higher than the former value. Such pronounced substrate roughness along with the presence of caverns in the size range of 1 μm (see the arrows in Figure 5c, d) could give rise to the Pb-Pt interfacial phase segregation promoted by the action of capillary forces, c.f. Figure 3 b, d. In the case of the optically-polished Pt-flat substrate surface, the intermetallic phase is distributed evenly and forms a continuous layer at the film/substrate interface, c.f. Figure 3 a, c.

Further, we investigated the ferroelectric properties of 0.65PMN–0.35PT films on both Pt substrates. The polarisation - electric field hysteresis loops of the films are shown in Fig 6. The coercive electric field (E_c) is in both cases similar, around 15 kV/cm. However, the values of the remnant polarization (P_r) of the films on Pt-flat and Pt-rough substrates are 27 and 15 $\mu\text{C}/\text{cm}^2$, respectively. This means that the higher remnant polarization coincides with the higher degree of (001) domain orientation. Such relation was found in the study of the domain structure in tetragonal 0.62PMN–0.38PT single crystals, where the spontaneous polarization is along the (001) direction. The P_r along (001) direction was 37 $\mu\text{C}/\text{cm}^2$, while it was much lower along the non-polar (111) direction, around 20 $\mu\text{C}/\text{cm}^2$ [20].

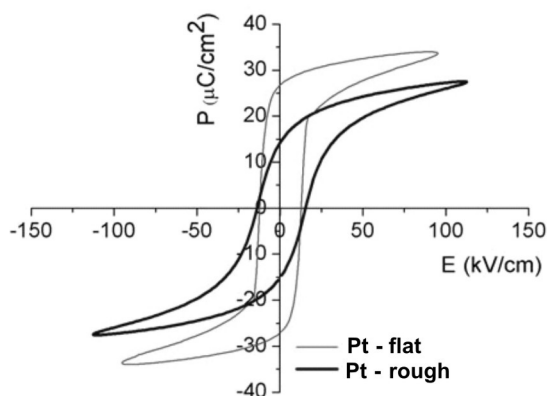


Figure 6: Polarisation – electric field hysteresis loops of the 0.65PMN–0.35PT thick films on Pt-flat and Pt-rough substrates.

4 Conclusions

In this work the influence of the roughness of the Pt-substrate on the structural and ferroelectric properties of 0.65PMN–0.35PT thick films was discussed. The thick-films were deposited on the Pt substrates with

very different roughnesses. The optically-polished Pt-substrate revealed a smooth, flat surface with an rms roughness of 44 nm. In contrary; the Pt-substrate with an additional screen-printed Pt-layer had a rough surface with an rms roughness of 342 nm.

Transmission electron microscope analysis revealed the presence of a Pb-Pt layer at the film/substrate interface in both cases. This intermetallic phase was presumably formed as a consequence of a partial reduction of Pb^{2+} during the thermal decomposition of organic additives in the screen-printed film upon heating. The choice of the substrate markedly influenced the distribution of the interfacial layer: on the flat substrate, it was in a form of a continuous layer, while on the rough substrate it formed pockets.

The 0.65PMN–0.35PT film, deposited on the flat Pt substrate, revealed a larger degree of the (001) domain orientation of the tetragonal phase than the film, deposited on the rough substrate. Consequently the remnant polarization (P_r) of the former film was higher, i.e., 27 $\mu\text{C}/\text{cm}^2$, than of the latter film, i.e., 15 $\mu\text{C}/\text{cm}^2$. The work demonstrates that the surface properties of the platinum substrate and related film/substrate interface reactions may significantly influence structure and ferroelectric properties of thick films.

5 Acknowledgement

The authors thank Brigita Kmet and Jena Cilenšek for help in the experimental work. The research was funded by the Slovenian Research Agency (Project J2-3633-1000-10-213633, *Textured ceramic films for sensors and actuators* and Program P2-0105 *Electronic Ceramics, Nano-, 2D and 3D Structures*).

6 References

1. Park, S. E.; Shrout, T. R., *J. Appl. Phys.* 1997, 82, 1804.
2. Heartling, G. H., *J. Am. Ceram. Soc.* 1999, 82, 797.
3. Uršič, H.; Kosec, M., *Relaxor-ferroelectric PMN–PT thick films*. V: LALLART, Mickaël (ur.). *Ferroelectrics - physical effects*. Rijeka: InTech, cop. 2011, pp. 27–48.
4. Uršič, H.; Hrovat, M.; Holc, J.; Zarnik, S. M.; Drnovšek, S.; Maček, S. *Sensors Actuat. B* 2008, 133, 699.
5. Uršič, H.; Hrovat, M.; Holc, J.; Tellier, J.; Drnovšek, S.; Guiblin, N.; Dkhil, B.; Kosec, M., *J. Eur. Ceram. Soc.* 2010, 30, 2081.
6. Kosec, M.; Holc, J.; Kuščer, D.; Drnovšek, S., *J. Eur. Ceram. Soc.* 2007, 27, 3775.

7. Kuščer, D.; Holc, J.; Kosec, M., *J. Am. Ceram. Soc.* 2007, 90, 29.
8. Kosec, M.; Uršič, H.; Holc, J.; Hrovat, M.; Kuščer, D.; Malič B., *IEEE Trans. Ultrason., Ferroelectr., Freq. Control* 2010, 57, 2205.
9. Petricek, V.; Dusek, M.; Palatinus, L., *Jana2006. The crystallographic computing system, Institute of Physics, Praha, Czech Republic, (2006).*
10. Singh, A. K.; Pandey, D., *Phys. Rev. B* 2003, 67, 064102-1.
11. Brooks, K. G.; Reaney, I. M.; Klissurska, R.; Huang, Y.; Bursill, L.; Setter, N., *J. Mater. Res.* 1994, 9, 2540.
12. Chen, S. Y.; Chen, I. W., *J. Amer. Ceram. Soc.* 1994, 77, 2332.
13. Impey, S. A.; Huang, Z.; Patel, A.; Beanland, R.; Shorrocks, N. M.; Watton, R.; Whatmore, R. W., *J. Appl. Phys.* 1998, 83, 2202.
14. Huang, Z.; Zhang, Q.; Whatmore, R. W., *J. Appl. Phys.* 1999, 85, 1157.
15. Mandeljc, M.; Malič, B.; Kosec, M.; Dražič, G., *Mater. Res. Soc. Symp. Proc.* 2006, Vol. 902E, Materials Research Society 0902-T03-37.1
16. Malič, B.; Mandeljc, M.; Dražič, G.; Škarabot, M.; Mušević, I.; Kosec, M., *Integrated Ferroelectrics* 2008, 100, 285.
17. Lee, J. K.; Jung, H. S.; Kim, D. W.; Kim, C. H.; Hong, K. S., *J. Mater. Res.* 2002, 17, 1030.
18. Haigh, R. D.; Whatmore, R. W., *Sensors Actuat. A*, 2009, 151, 203.
19. Massalski, T. B., Murray, J. L., Bennett, L. H., Baker, H., *Binary Alloy Phase Diagrams*, American Society for Metals, Metals Park, 44073 Ohio, USA, Second addition 1987, pp. 1837.
20. Feng, Z.; Zhao, X.; Luo, H., *J. Phys.: Condens. Matter.* 2004, 16, 3769.

Arrived: 25. 07. 2013

Accepted: 19. 01. 2014